Inventory of Supplemental Materials.

Supplemental Figures:

Figure S1. Related to Figure 1. RavZ N-terminal domain is structurally homologous to the Ulp family of Ubl deconjugating enzymes. RavZ deconjugation activity assay.

Figure S2. Related to Figure 2. RavZ protease activity requires α3 but not high affinity membrane interactions. RavZ deconjugation activity assay.

Figure S3. Related to Figure 2. Determination of liposome size.

Supplemental Tables:

Table S1. Related to Figure 1. Crystallographic Statistics.

Table S2. Related to Figure 2. Statistical analysis of Figure 2.

Table S3. Related to Figure 3. Statistical analysis of Figure 3C.

Supplemental Experimental Procedures

Protein Expression and Isolation

Protein Crystallization and Structure Determination

Structural homology search

Liposome preparation

Negative stain electron microscopy of liposomes

Delipidation assay

RavZ Binding

Imaging

LC3 puncta formation in macrophages infected with L. pneumophila

Statistics

Supplemental References

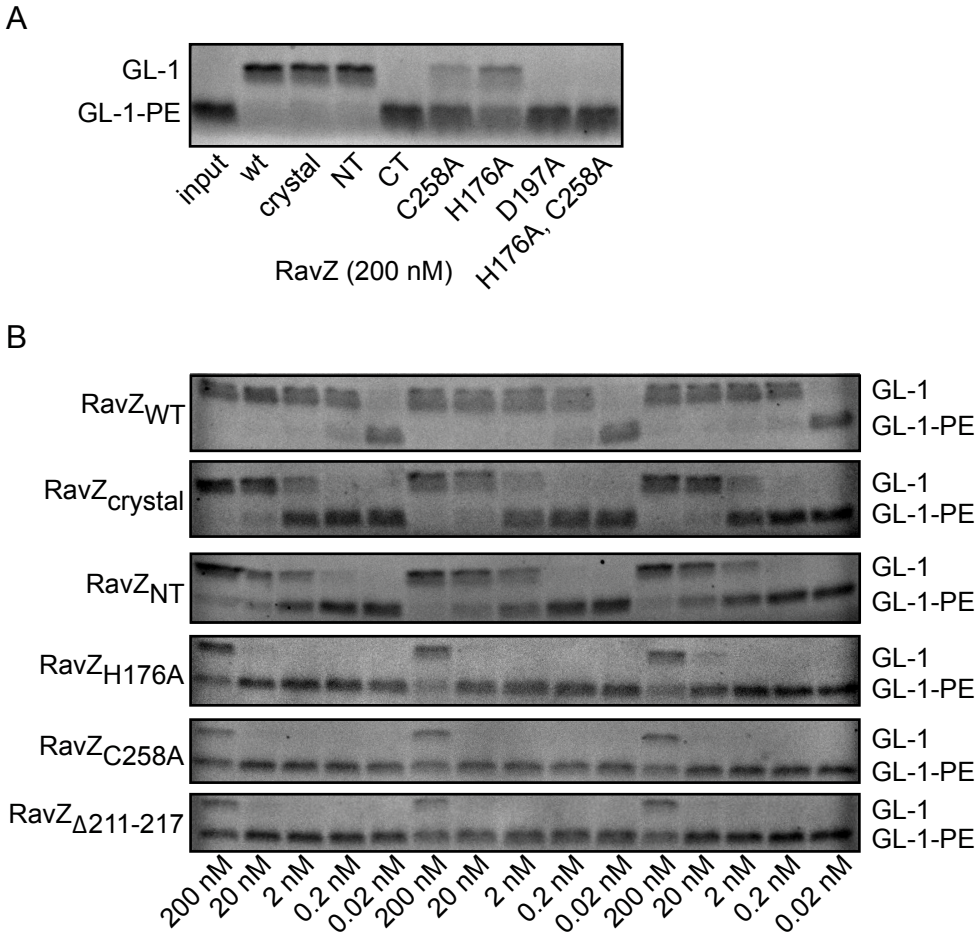

Figure S1. Related to Figure 1. RavZ deconjugation activity assay. Free GL-1 migrates more slowly in SDS-PAGE than PE conjugated GL-1. (A) SDS-PAGE of GL-1-PE (10 μM) on 25 nm liposomes (DOPE:DOPC:blPI in a 55:35:10 molar ratio) after incubation for 1 h at room temperature with $RavZ_{WT}$ or RavZ mutants (200 nM). Gels were stained with Coomassie dye. (B) SDS-PAGE of GL-1-PE (10 μM) after incubation for 1 h at room temperature with $RavZ_{WT}$ or RavZ mutants (0.02 to 200 nM). Gels were stained with Coomassie dye. Quantification of deconjugated GL-1 relative to total GL-1 shown in **Figure 1B**.

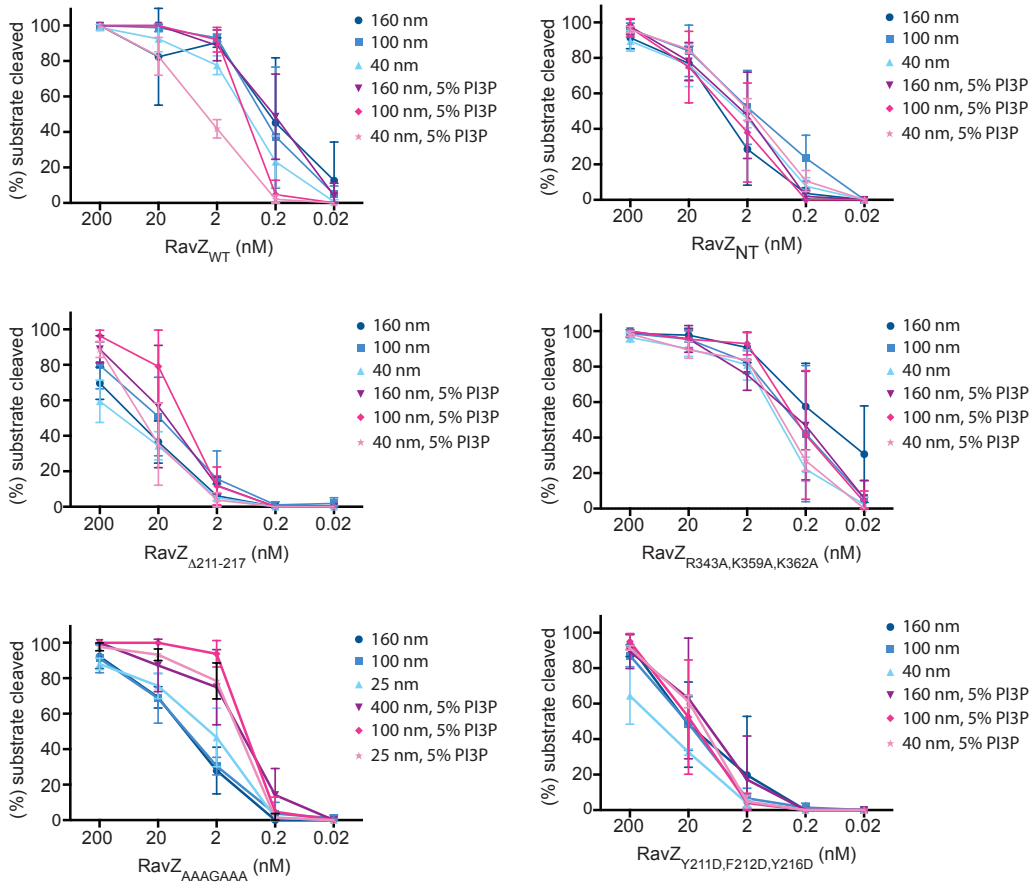

Figure S2. Related to Figure 2. RavZ protease activity requires α3 but not high affinity membrane interactions. RavZ deconjugation activity assay. GL-1-PE (10 μM) on liposomes either with 5% PI3P (DOPE:DOPC:blPI:PI3P in a 30:55:10:5 molar ratio) or without (DOPE:DOPC:blPI in a 30:60:10 molar ratio) was incubated for 1 h at room temperature with $RavZ_{WT}$ or RavZ mutants (0.02 nM to 200 nM). Liposome composition was identical to (**Figure 2D**) to ensure comparability. The amount of deconjugated GL-1 relative to total GL-1 was quantified. Depicted are the mean and standard deviation of three independent experiments. The results for all RavZ mutants at 2 nM concentration have been depicted in **Figure 2E**.

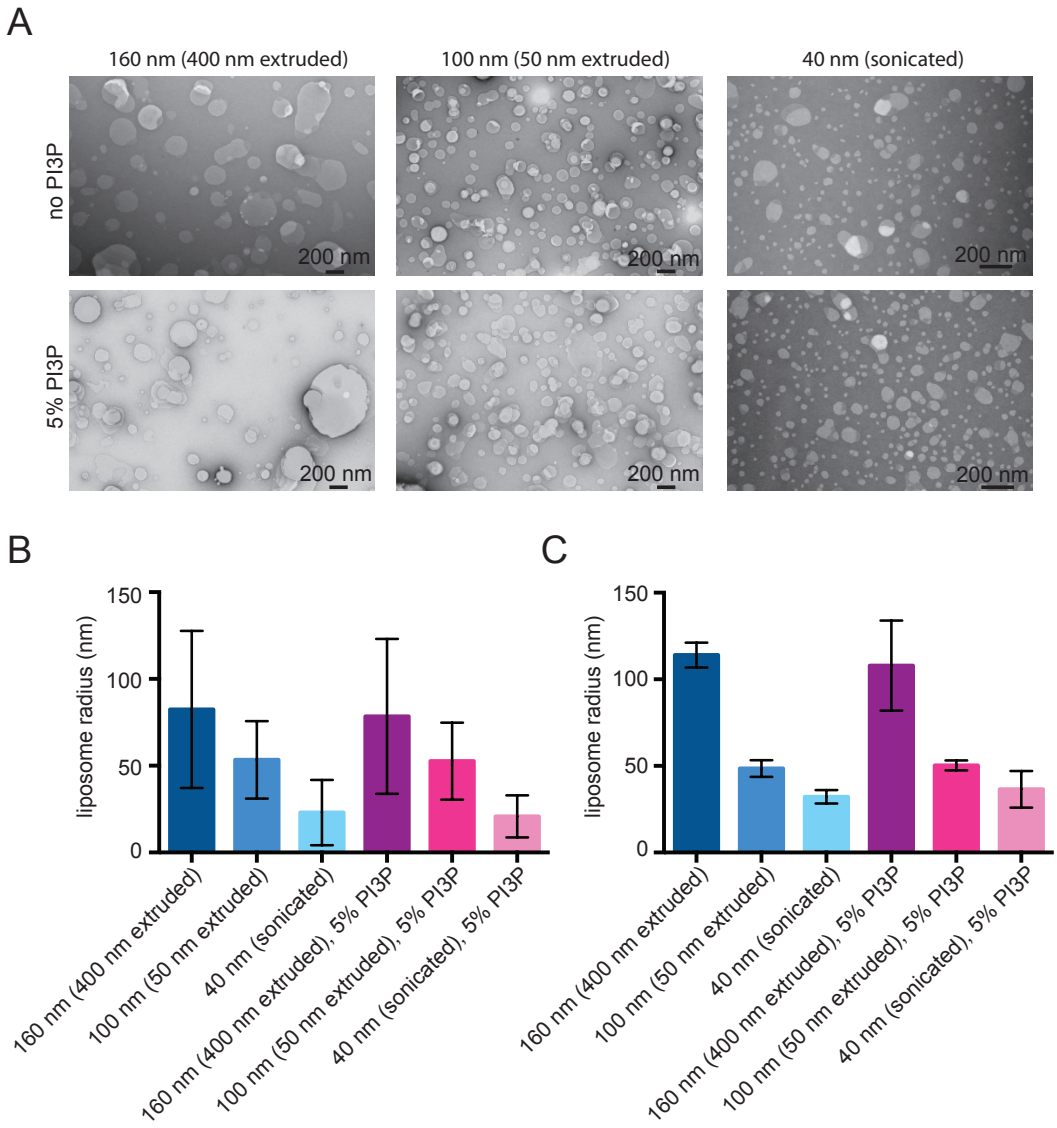

Figure S3. Related to Figure 2. Determination of liposome size. Liposomes for RavZ binding assays (**Figure 2D**) and RavZ delipidation activity assays (**Figure 2E**) were prepared by extrusion through 400 nm and 50 nm filters as well as sonication. For the first preparation of liposomes the actual size was determined by negative stain electron microscopy (EM). Dynamic light scattering (DLS) was used to monitor consistency in size between all liposome preparations used. (A) Negative stain EM images of liposomes used for experiments depicted in **Figure 2E** and **2D.** (B) Average radius (mean ± SD) of

liposomes used for experiments depicted in **Figure 2E** and **2D** determined by negative stain EM. (C) Average liposome radius (mean ± SD) of all liposome preparations used for experiments depicted in **Figure 2E** and **2D** as determined by DLS.

Supplemental Tables:

Table S1. Related to Figure 1. Crystallographic Statistics		
Data Collection		
	native	Se-substituted
Space group	I422	I422
Unit cell dimensions (a, b, c in Å; α, β, γ in °)	221.78, 221.78, 72.54 90, 90, 90	221.78, 221.78, 73.21 90, 90, 90
Wavelength (Å)	0.9792	0.9792
Resolution (Å)	110.9-2.98 (3.14-2.98)	156.96–3.28 (3.46–3.28)
R_{merge}	0.066 (2.396)	0.145 (2.93)
I/σ	17.6 (0.9)	32.4 (1.7)
Completeness (%)	99.2 (98.2)	100.0 (100.0)
Redundancy	5.7 (5.9)	31.1 (29.1)
Refinement		
Resolution (Å)	68.96-2.98 (3.07-2.98)	–
No. of unique reflections	18179	–
R_{work}/R_{free} (%) [b]	21.43/25.04	–
No. of protein atoms	2608	–
Average B ($Å^2$)	122	–
Rmsd		
Bond length (Å)	0.009	–
Bond angle (°)	1.33	–
Ramachandran plot[d]		
Favoured (% residues)	96	–
Allowed (% residues)	4	–
Disallowed (% residues)	0	–

Table S2. Related to Figure 2. Statistical analysis of Figure 2. The data presented in **Figure 2A, 2C, 2D and 2E** has been analyzed by one-way (**Figure 2A and 2C**) or two-way ANOVA (**Figure 2D and 2E**) and has been found to contain significant differences. The table shows the results of the *post-hoc* comparisons of all means of one experiment with each other using Tukey's method. Presented are the mean difference (mean Diff.), 95% confidence interval of mean difference (95% CI diff.) and the multiplicity-adjusted p-value (Adjusted P-value) of all comparisons. *: p-value < 0.05. **; p-value < 0.01. ***; p-value < 0.001. ****; p-value < 0.0001. **Tab1:** Statistical analysis of Figure 2A. **Tab 2:** Statistical analysis of Figure 2C. T**ab 3:** Statistical analysis of Figure 2D. **Tab 4:** Statistical analysis of Figure 2E.

See separate Excel file: Table S2.xlsx

Table S3. Related to Figure 3. Statistical analysis of Figure 3C. The data presented in **Figure 3C** has been analyzed by one-way ANOVA and has been found to contain significant differences. The table shows the results of the *post-hoc* comparisons of all means in **Figure 3C** with each other using Tukey's method. Presented are the mean difference (mean Diff.), 95% confidence interval of mean difference (95% CI diff.) and the multiplicity-adjusted p-value (Adjusted p-value) of all comparisons. ns: not significant. *: p-value < 0.05. **: p-value < 0.01. ***: p-value < 0.001. ****: p-value < 0.0001.

Comparison	Mean Diff.	95% CI of diff.	Adjusted p-value	Summary
uninfected vs. Δ*ravz*	4.65	-10.07 to 19.37	0.8318	ns
uninfected vs. $RavZ_{WT}$	62.2	47.48 to 76.91	< 0.0001	****
uninfected vs. $RavZ_{R343A, K359A, K362A}$	20.51	5.787 to 35.23	0.0069	**
uninfected vs. $RavZ_{\Delta211-217}$	7.973	-6.747 to 22.69	0.4325	ns
Δ*ravz* vs. $RavZ_{WT}$	57.55	42.83 to 72.26	< 0.0001	****
Δ*ravz* vs. $RavZ_{R343A, K359A, K362A}$	15.86	1.137 to 30.58	0.0337	*
Δ*ravz* vs. $RavZ_{\Delta211-217}$	3.323	-11.40 to 18.04	0.9411	ns
$RavZ_{WT}$ vs. $RavZ_{R343A, K359A, K362A}$	-41.69	-56.41 to -26.97	< 0.0001	****
$RavZ_{WT}$ vs. $RavZ_{\Delta211-217}$	-54.22	-68.94 to -39.50	< 0.0001	****
$RavZ_{R343A, K359A, K362A}$ vs. $RavZ_{\Delta211-217}$	-12.53	-27.25 to 2.187	0.1061	ns

Supplemental Experimental Procedures

Protein Expression and Isolation. Recombinant RavZ constructs and GL-1 (residues 1-116) were expressed in E. coli BL21(DE3) cells as GST-fusion proteins with a PreScission protease cleavage site after the GST-tag. Cells were grown at 37°C to an OD_{600} of 0.6, protein expression was induced by the addition of 0.3 mM IPTG, and the temperature was lowered to 25°C. Cells were harvested 20 h after induction. For structure determination, selenomethionine substituted $RavZ_{crystal}$ (residues 10-458, Δ23-43, Δ430-440) was expressed similarly according to (Budisa et al., 1995). Cells were collected by centrifugation and resuspended in lysis buffer (20 mM Hepes pH 7.8, 100 mM NaCl, 1 mM PMSF, 1 mM TCEP). After cell lysis using a cell disruptor (Avestin), lysates were cleared by centrifugation and the GST-fusion proteins isolated by affinity chromatography using glutathione-sepharose 4B resin (GE Life Science). The proteins were eluted by overnight on-column cleavage with PreScission protease at 4°C. RavZ constructs for crystallization were further purified by size exclusion chromatography (Superdex S200 16/60) in 20 mM Hepes pH 7.8, 100 mM NaCl, 2 mM TCEP and concentrated to ~40 mg/ml.

ATG7 and ATG3 were expressed and isolated as described previously (Nath et al., 2014).

Protein Crystallization and Structure Determination. Crystals were grown at 4°C using the hanging drop vapor diffusion method, mixing equal volumes of $RavZ_{crystal}$ (40 mg/ml) and reservoir solution (0.1 M MES pH 5.1, 12% PEG 3350, 0.2 M $BaCl_2$). For cryo-protection, crystals were transferred step-wise to mother liquor solutions supplemented with increasing amounts of glycerol (5%, 10%, 15%, 20%), loop mounted, and flash frozen in liquid nitrogen.

Diffraction data were collected at beam line NE-CAT 24-ID-C at APS Argonne National Laboratory and processed using XDS (Kabsch, 1993). An initial low-resolution structure was solved by single anomalous wavelength dispersion method (SAD) at the selenium edge using data from a selenomethionine-substituted crystal (Hendrickson, 1991). We identified the selenium positions and additionally one barium position, calculated experimental phases and density modified maps, and built an initial model using the phenix AutoSol pipeline (Adams et al., 2010). This structure was used for phasing of a higher resolution native dataset by molecular replacement (Rossmann, 1972) using phaser (McCoy et al., 2007). After initial simulated annealing (torsion angle) in phenix.refine (Adams et al., 2010), the model was refined by multiple iterations of manual model rebuilding in coot (Emsley and Cowtan, 2004) followed by positional and Translation-Libration-Screwmotion (TLS) refinement with phenix.refine (Adams et al., 2010). Figures were made using PyMOL (The PyMOL Molecular Graphics System). The electrostatic surface potential was calculated using APBS (Baker et al., 2001).

Structural homology search. To identify structurally homologous proteins we used the protein structure comparison server Fold at European Bioinformatics Institute (http://www.ebi.ac.uk/msd-srv/ssm) (Krissinel and Henrick, 2004).

Liposome preparation. To prepare liposomes for use in delipidation and liposome binding assays, different molar ratios of dioleyoyl-phosphatidylethanolamine (DOPE), palmitoyl-oleyl-phosphatidylcholine (POPC), phosphatidylinositol from bovine liver (blPI), DOPE-Rhodamine and the phosphatidylinositol phosphates (PIPs) were mixed in chloroform and dried to a thin film. The lipids were reconstituted in a buffer containing 20 mM Tris, pH 7.6, 100 mM NaCl. Note that in

experiments where RavZ binding was directly compared to RavZ activity (i.e. Figure 2D and 2E and Figure S2), 5 mM MgCl2 was also included in the buffer. The reconstituted lipids were exposed to 7 cycles of flash freezing in liquid nitrogen and thawing in a 37°C water bath. 400 nm and 50 nm extruded liposomes were prepared by extruding the frozen/thawed lipid mixtures through two polycarbonate filters with 400 nm and 50 nm pores a total of 21 times. To prepare very small liposomes, 400 nm liposomes were sonicated. Liposome size was assessed using Dynamic Light Scattering (DLS, DynaPro NanoStar from Wyatt Technology, running Dynamics (7.1.7)) and negative staining electron microscopy (JEOL JEM-1400plus, operated at 80 kV) (**Fig. S3**). The composition and size of liposomes used for any individual experiment is as indicated in the respective Figure or Figure legend, except that all liposomes contain 0.5% DOPE-Rhodamine, replacing an equivalent amount of POPC, for quantification purposes.

Negative stain electron microscopy of liposomes. For negative staining transmission electron microscopy (TEM), a drop of sample (~5 µL) was deposited on a glow discharged formvar/carbon coated copper grid (Electron Microscopy Sciences), incubated for 1-3 minute and blotted away. The grid was then washed briefly and stained for 1 minute with 2% (w/v) uranyl formate. Images were acquired on a JEOL JEM-1400 Plus microscope (acceleration voltage: 80 keV) with a bottom-mount 4k×3k CCD camera (Advanced Microscopy Technologies).

Delipidation assay. GL-1 was coupled to PE as described previously (Jotwani et al., 2012). Briefly, GL-1 (15 µM), Atg3 (3 µM), Atg7 (3 µM), and liposomes (3 mM lipid) were mixed in a buffer containing 20 mM Tris, pH 7.6, 100 mM NaCl, 5 mM MgCl2, 1 mM DTT. Lipidation was initiated by the addition of 1 mM ATP and the samples

were incubated at 37°C for 2 h. Completed reactions were stored on ice before being applied to a nycodenz gradient to separate lipidated GL-1 from unlipidated GL-1 and other reaction components. The bottom layer of the gradient was formed by mixing the finished lipidation reactions 1:1 with 80% nycodenz. This 40% nycodenz mixture (350 µl) was followed by a 30% nycodenz (250 µl) and 0% nycodenz layer (50 µl; each nycodenz solution made up in reaction buffer). The samples were centrifuged for 4 hours at 48000 rpm in an SW-55 Beckman rotor. GL-1-PE liposomes were recovered from a tight band at the 0%/30% nycodenz interface.

Free GL-1 migrates more slowly in SDS-PAGE than PE conjugated GL-1, allowing for the detection of RavZ dependent GL-1-PE deconjugation by SDS-PAGE. Full-length, wild type RavZ ($RavZ_{WT}$, at 0.02 nM) still displayed measurable RavZ GL-1-PE conversion activity after incubation with GL-1-PE (10 µM) for 1 h at room temperature. To test RavZ mutants for activity, we initially tested them at high concentration (200 nM). To approximate the degree by which delipidation activity is reduced relative to the wild-type protein in RavZ mutants with residual activity, we determined the lowest concentration with measurable activity (in ten-fold dilution steps). Conversion of 20 µM GL-1-PE after 1 h at room temperature was measured at 200 nM, 20 nM, 2 nM, 0.2 nM and 0.02 nM RavZ mutant concentration. Gels were stained by Coomassie dye and scanned, and the amounts of GL-1 and PE-GL-1 were quantified using the ImageJ software (Schneider et al., 2012). The percentage of cleaved substrate (GL-1) relative to total substrate (GL-1 + PE-GL-1) was calculated.

RavZ Binding. WT or mutant RavZ (10 µM) was incubated with 2 mM total lipid and 1mM DTT in SN2 buffer (20 mM Tris pH 7.6, 100 mM NaCl) for 20 minutes at 37°C. Note that in experiments where RavZ binding was directly compared to RavZ

activity (i.e. Figure 2D, 2E and Figure S2), 5 mM MgCl2 was also included in the buffer. To separate liposomes and bound RavZ from free protein, this mixture was then subjected to a Nycodenz liposome flotation assay as described in (Nath et al., 2014). Gradients were centrifuged at 48,000 rpm in a sw55Ti rotor (Beckman) for 4 hours at 4°C. The liposomes and bound protein were recovered from the top 80 µl of the gradient. The lipid recovery from the gradient was determined by measuring DOPE-Rhodamine fluorescence using a SpectraMax fluorescence spectrometer. To determine the percentage of bound protein, 1/8 of the volume of the recovered liposomes and 1/20 of the initial amount of RavZ protein in the binding assay were run in precast 12% bis-Tris gels (Novex) running in 1X MES SDS Running Buffer (NuPage, Invitrogen). The protein was visualized with Coomassie Blue stain per the manufacturer's instruction (Imperial Protein Stain, Thermo Scientific). Gels were then visualized using the VersaDoc Imager (exposure time 0.5 sec) and analyzed through densitometry using ImageJ software. The resulting densitometry was normalized to the recovered total lipid.

Imaging. HeLa cells were plated at a density of 5x10^4 cells per well on coverslips in a 24-well plate. After 24 hours cells were transfected with 250 ng plasmid DNA per well using XtremeGene transfection reagent (Roche). Cells were fixed with 4% PFA 18 hours after transfection and then blocked and permeabilized in blocking buffer (2% BSA with 0.5% saponin). Cells were stained with rabbit anti-Atg16 antibody (MBL) diluted 1:100, and mouse anti-FLAG (M2) antibody (Sigma) diluted 1:500, in blocking buffer. Secondary antibodies, Alexa Fluor 568 and 488 (Life Technologies), were diluted 1:2000 in blocking buffer. Coverslips were mounted on slides with ProLong Gold Antifade reagent (Life Technologies). Images were acquired on

a Nikon Eclipse TE-2000S microscope with a 100x/1.4 numerical aperture objective lens and running SlideBook 6.0 software.

LC3 puncta formation in macrophages infected with L. pneumophila. The forward oligonucleotide 5'-cgcccgggatccttatgaaaggcaagttaacaggtaa-3' and reverse oligonucleotide 5'-cgatatctgcagctattttaccttaatgccaccat-3' were used to amplify mutant *ravZ* alleles to generate the plasmids pJB::RavZ$_{1\text{-}502}$, pJB::RavZ$_{\Delta 211\text{-}217}$, and pJB::RavZ$_{K359A,R343A,K362A}$. The amplified *ravZ* genes were ligated into pJB1806 (Bardill et al., 2005) that had been digested with BamHI and PstI, and the corresponding plasmids were electroporated into the *L. pneumophila* Δ*ravZ* mutant CR1925 (Choy et al., 2012). Transformants were grown at 37^{o}C and selected on CYE plates containing 10 μg/ml of chloramphenicol. Bone marrow macrophages (BMDMs) were derived from NLRC4-/- mice and infected with *L. pneumophila* as described previously (Zamboni et al., 2006). Briefly, BMDMs were cultured in 24-well plates on glass coverslips at a density of 7x10^{4} and infected with *L. pneumophila* at a multiplicity of infection of 10. Infected cells were treated with 10 μg/ml of Bafilomycin A1 (Sigma) at 30-minutes post-infection to prevent LC3 degradation in autolysosomes and fixed at 2-hours post-infection in 4% paraformaldehyde in PBS. Fixed cells were permeabilized for 5-seconds in ice-cold 100% methanol. Cells were stained with a rabbit polyclonal antibody specific for *L. pneumophila* diluted 1:1000 and a mouse monoclonal antibody specific for LC3 (NanoTools) diluted 1:200. The secondary antibodies Alexafluor 568 goat anti-rabbit (Invitrogen) and Alexa Fluor 488 goat anti-mouse (Invitrogen) were used at 1:1000 and DNA was stained using 0.1 μg/ml of Hoescht for 10 minutes. Coverslips were mounted onto glass slides using ProLong Gold (Life Technologies). Fluorescence microscopy was used to

evaluate infected cells for LC3-positive *puncta*. Cells were scored positive for LC3 *puncta* formation if they displayed LC3-positive structures that were similar to those found in uninfected control cells. Three independent assays were conducted in which 100 infected cells were scored for each strain tested. Digital images were acquired with a Nikon Eclipse TE2000-S inverted fluorescence microscope equipped with a Nikon Plan Apo 60X 1.4 NA lens and a Photometrics CoolSNAP EZ camera controlled by SlideBook v.5.5 imaging software.

Supplemental References

Adams, P.D., Afonine, P.V., Bunkoczi, G., Chen, V.B., Davis, I.W., Echols, N., Headd, J.J., Hung, L.W., Kapral, G.J., Grosse-Kunstleve, R.W., *et al.* (2010). PHENIX: a comprehensive Python-based system for macromolecular structure solution. Acta crystallographica Section D, Biological crystallography *66*, 213-221.

Baker, N.A., Sept, D., Joseph, S., Holst, M.J., and McCammon, J.A. (2001). Electrostatics of nanosystems: application to microtubules and the ribosome. Proceedings of the National Academy of Sciences of the United States of America *98*, 10037-10041.

Bardill, J.P., Miller, J.L., and Vogel, J.P. (2005). IcmS-dependent translocation of SdeA into macrophages by the Legionella pneumophila type IV secretion system. Molecular microbiology *56*, 90-103.

Budisa, N., Steipe, B., Demange, P., Eckerskorn, C., Kellermann, J., and Huber, R. (1995). High-level biosynthetic substitution of methionine in proteins by its analogs 2-aminohexanoic acid, selenomethionine, telluromethionine and ethionine in Escherichia coli. European journal of biochemistry / FEBS *230*, 788-796.

Choy, A., Dancourt, J., Mugo, B., O'Connor, T.J., Isberg, R.R., Melia, T.J., and Roy, C.R. (2012). The Legionella effector RavZ inhibits host autophagy through irreversible Atg8 deconjugation. Science *338*, 1072-1076.

Emsley, P., and Cowtan, K. (2004). Coot: model-building tools for molecular graphics. Acta Crystallographica Section D-Biological Crystallography *60*, 2126-2132.

Hendrickson, W.A. (1991). Determination of macromolecular structures from anomalous diffraction of synchrotron radiation. Science *254*, 51-58.

Jotwani, A., Richerson, D.N., Motta, I., Julca-Zevallos, O., and Melia, T.J. (2012). Approaches to the study of Atg8-mediated membrane dynamics in vitro. Methods in cell biology *108*, 93-116.

Kabsch, W. (1993). Automatic Processing of Rotation Diffraction Data from Crystals of Initially Unknown Symmetry and Cell Constants. J Appl Crystallogr *26*, 795-800.

Krissinel, E., and Henrick, K. (2004). Secondary-structure matching (SSM), a new tool for fast protein structure alignment in three dimensions. Acta crystallographica Section D, Biological crystallography *60*, 2256-2268.

McCoy, A.J., Grosse-Kunstleve, R.W., Adams, P.D., Winn, M.D., Storoni, L.C., and Read, R.J. (2007). Phaser crystallographic software. J Appl Crystallogr *40*, 658-674.

Nath, S., Dancourt, J., Shteyn, V., Puente, G., Fong, W.M., Nag, S., Bewersdorf, J., Yamamoto, A., Antonny, B., and Melia, T.J. (2014). Lipidation of the LC3/GABARAP

family of autophagy proteins relies on a membrane-curvature-sensing domain in Atg3. Nature cell biology *16*, 415-424.
Rossmann, M.G. (1972). The molecular replacement method; a collection of papers on the use of non-crystallographic symmetry (New York,: Gordon and Breach).
Schneider, C.A., Rasband, W.S., and Eliceiri, K.W. (2012). NIH Image to ImageJ: 25 years of image analysis. Nature methods *9*, 671-675.
The PyMOL Molecular Graphics System, V.S., LLC. The PyMOL Molecular Graphics System, Version 1.5.0.4 Schrödinger, LLC.
Zamboni, D.S., Kobayashi, K.S., Kohlsdorf, T., Ogura, Y., Long, E.M., Vance, R.E., Kuida, K., Mariathasan, S., Dixit, V.M., Flavell, R.A.*, et al.* (2006). The Birc1e cytosolic pattern-recognition receptor contributes to the detection and control of Legionella pneumophila infection. Nature immunology *7*, 318-325.